PART IV

SYSTEMS

Magnetic Actuators and Sensors, Second Edition. John R. Brauer.

CHAPTER 12

Coil Design and Temperature Calculations

Magnetic actuators and sensors are often components of large systems, such as automobiles. The actuators and sensors must perform reliably in the system environment and interface properly with the system.

To interface properly with system power supplies, the coils of the magnetic components must be properly designed, as described in this chapter. As part of the coil design, the temperatures developed by the coils and the components must be predicted. The relationship between electromagnetics (EM) and temperatures T is shown in Figure 12.1 as a block diagram.

12.1 WIRE SIZE DETERMINATION FOR DC CURRENTS

Many DC power supplies consist of a fixed voltage. For example, automobiles have a standard 12 V supply, although the voltage under no load is actually 14 V, and other higher voltages are being added to accommodate ever-growing electrical demands.

As discussed in Chapter 7 and other previous chapters, the magnetic field and force are determined by ampere-turns NI. Ampere's law states that NI produces the field, not voltage. Thus the engineer designing a magnetic actuator or sensor must ensure that the coil carries the proper NI.

For DC voltages V, Ohm's law gives the relation between V and current I:

$$I = V/R \tag{12.1}$$

where R is the coil resistance in ohms. Similar to reluctance of Chapter 3 and as depicted in Figure 3.2, resistance is related to geometry:

$$R = l/(\sigma S_c) \tag{12.2}$$

where l is length of the conducting coil wire, σ is its conductivity, and S_c is the cross-sectional area of the wire.

Magnetic Actuators and Sensors, Second Edition. John R. Brauer.

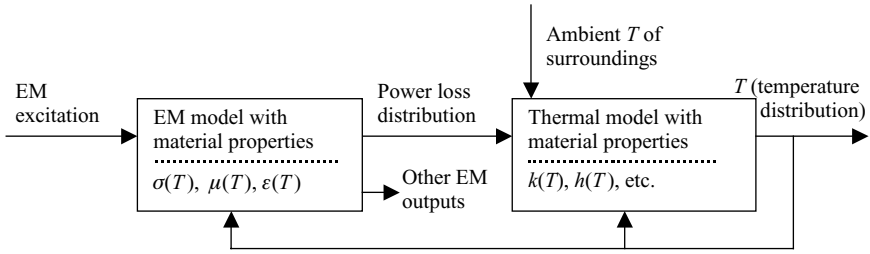

FIGURE 12.1 Modeling temperature and its effects in magnetic devices, to be discussed in this chapter.

For copper at room temperature (20°C), σ is 5.8E7 S/m. The other common coil material, aluminum, has a room temperature conductivity of approximately 3.6E7 S/m. Both materials, however, change their conductivity with temperature T, as indicated in Figure 12.1. For $0 < T < 100$°C, the conductivity of copper obeys:

$$\sigma = \frac{5.8\text{E7 S/m}}{1 + 0.00393(T - 20^{\circ}\text{C})} \tag{12.3}$$

That is, the conductivity of copper decreases by approximately 0.4% for each degree Celsius rise in temperature. The resistivity of copper, being the reciprocal of conductivity, increases with temperature, having a positive temperature coefficient.

While square or rectangular wire is sometimes used, usually the wire used to wind coils has a circular cross section. Thus its cross-sectional area S_c is related to wire diameter d:

$$S_c = \pi r^2 = \pi d^2/4 \tag{12.4}$$

Instead of choosing any wire diameter, one chooses an available *wire gauge*. Different countries can use different gauges. The American Wire Gauge (AWG) is a number, usually an integer, that gives the bare wire diameter [1]:

$$d = (0.00826)(1.123^{-\text{AWG}})\ \text{m} \tag{12.5}$$

In AWG, every 6-gauge decrease gives a doubling of the wire diameter, and every 3-gauge decrease gives a doubling of the cross-sectional area of the wire. Also common is the metric wire gauge, which is simply 10 times the diameter in millimeters. Thus increasing wire size is accomplished by decreasing AWG or by increasing metric gauge.

However, all wires require insulation. The insulation can be a very thin enamel or other coating, consisting of one or more layers called *builds*. One can consult wire tables to determine insulated wire diameters.

The coil occupies a given coil winding area, as shown for example in any of the DC actuators of Chapter 7. The relation between the coil winding area S_w and the

copper (or other wire material) area is the *packing factor*:

$$F_p = NS_c/S_w \tag{12.6}$$

For circular wires, even when they are tightly wound, the packing factor is typically only about 75%. Conservative designs assume a maximum $F_p = 0.70$ or less [1].

Based on the above equations, various coil design procedures can be followed. Given a certain winding area and voltage, the desired NI can be obtained. However, if I is too high a value, then the coil temperature may become too high [2], as will be discussed later in this chapter. Maximum permissible current densities vary with cooling and other factors, but a reasonable value in some cases is 40 A/mm^2. All coil insulation is only capable of withstanding a certain temperature rise, for example, 40°C.

Example 12.1 Simple DC Coil Design at a Given Temperature An axisymmetric copper coil is to be designed to operate at a maximum temperature of 60°C. The available winding area S_w is 1.E−3 m^2 and the average coil radius is 5 cm. Assume a packing factor of 70% and a DC voltage of 12 V. If $NI = 1000$ ampere-turns, find the bare wire diameter, the number of turns N, and the current density.

Solution The length of a turn l_T is 2π times the 0.05-m radius, and thus $l_T =$ 0.31416 m. The conductivity σ of the copper at 60°C is found using (12.3) to be 5.012E7 S/m. This value can be used in the resistance equation from (12.2) and (12.4):

$$R = 4\frac{Nl_T}{\sigma\pi d^2} \tag{E12.1.1}$$

The other key equation, based on (12.1), is:

$$NI = NV/R \tag{E12.1.2}$$

Substituting (E12.1.1) and solving for the bare diameter gives:

$$d = \sqrt{\frac{4NIl_T}{\sigma F_P \pi V}} \tag{E12.1.3}$$

Inserting the known values of σ, F_P, V, l_T, and NI gives $d = 0.975$ mm. Then using (12.6):

$$N = F_p S_w/S_c = 4F_p S_w/(\pi d^2) \tag{E12.1.4}$$

Inserting the known values gives $N = 938$ turns. Thus each turn carries 1000/938 = 1.066 A. The current density is the current per unit area of copper, and here is 1.43 A/mm^2, a reasonably small value.

12.2 COIL TIME CONSTANT AND IMPEDANCE

In all DC and AC magnetic actuators and sensors, the time constant is important. When a DC voltage V is applied (as a step), the current rises exponentially according to:

$$I = \frac{V}{R}(1 - e^{-t/\tau_e}) \tag{12.7}$$

where the electric time constant $\tau_e = L/R$. When an AC voltage V_{AC} is applied, then (ignoring capacitive effects), the steady-state AC current obeys the complex phasor relation:

$$I_{\text{AC}} = \frac{V_{\text{AC}}}{Z} = \frac{V_{\text{AC}}}{R + j\omega L} \tag{12.8}$$

where Z is the complex AC impedance. Thus the current has the phase angle:

$$\theta_I = -\arctan(\omega L/R) \tag{12.9}$$

Hence the L/R ratio is important for both DC and AC magnetic devices.

One expects that the coil design would affect the L/R time constant and the impedance. Thus this section investigates the design of a coil in a given coil winding area S_w. We seek to choose N for minimum time constant L/R and minimum energy W lost in ohmic power in the coil. Inductance L, resistance R, and the related τ_e and W can be calculated for a coil of given area S_w and ampere-turns NI. The derivation that follows ignores velocity effects.

From Chapter 3, L is proportional to the square of N and to permeance P of (3.14):

$$L = N^2\mathcal{P} = (NI/I)^2\mathcal{P} = (NI)^2\mathcal{P}/(I^2) \tag{12.10}$$

Resistance R of the coil is proportional to length of wire (here N times the length of each turn l_T) divided by the product of conductivity and wire area times packing factor:

$$R = Nl_T/(\sigma F_p S_c/N) \tag{12.11}$$

$$R = N^2 l_T/(\sigma F_p S_c) \tag{12.12}$$

The related electric circuit time constant $\tau_e = L/R$ is then:

$$\tau_e = N^2\mathcal{P}/(\sigma F_p S_c)/(N^2 l_T) \tag{12.13}$$

$$\tau_e = \mathcal{P}(\sigma F_p S_c)/l_T \tag{12.14}$$

Thus the time constant L/R is independent of turns N.

Energy loss W (power loss integrated over time) is proportional to the square of I and to resistance:

$$W = kI^2R = k\,(NI/N)^2N^2l_T/(\sigma S_c F_p) \tag{12.15}$$

$$W = k(NI)^2 l_T/(\sigma S_c F_p) \tag{12.16}$$

Hence W depends (as would be expected) on excitation NI, but does not depend on whether the coil designer chooses a high N and low I or a low N and high I.

Thus the engineer designing a high speed actuator cannot vary N over a given area and expect the coil current rise time to be minimized. Instead, what must be done to reduce the time for the current to rise to a given amperage is to increase the voltage applied to the coil. This voltage increase is usually temporary to avoid excessive coil power loss and overheating.

For the Bessho actuator of Figure 5.2, the time constant τ_e is 20 ms [3]. The inductance computed by magnetostatic finite-element software [4] for a 10-mm airgap = 3.15 H, which then leads to a resistance $R = L/\tau_e = \sim 150\ \Omega$, which is believed to be close to the actual R [4]. Even if the number of turns were changed from the 3300 of Figure 5.2, the initial time constant would remain 20 ms.

12.3 SKIN EFFECTS AND PROXIMITY EFFECTS FOR AC CURRENTS

The above DC resistance R can be increased significantly under AC operation. From Faraday's law, the magnetic fields produced by the AC current induce additional AC currents in the coil conductors. These additional currents produce additional losses, and sometimes change the current density distribution from uniform to nonuniform.

The skin depth equation (8.1) of Chapter 8 applies not only to steel but to coil conductors, and is repeated here:

$$\delta = \frac{1}{\sqrt{\pi f \mu \sigma}} \tag{12.17}$$

where f is the AC frequency in Hz and σ is electrical conductivity. Coils of copper and aluminum have permeability $\mu = 12.57\text{E}{-7}$, the permeability of air. The derivation of the above skin depth assumes one-dimensional conducting slabs, but (12.17) is an approximate indicator of the depth of currents and magnetic fields for many practical problems.

When the skin depth is much greater than the wire radius, then AC magnetic flux density can be shown to produce losses similar to those of (8.2):

$$\frac{P_e}{v} = \frac{\omega^2\sigma}{24}\left(w_y^2 B_x^2 + w_x^2 B_y^2\right) \tag{12.18}$$

where B_x and B_y are components of the peak AC magnetic flux density passing through the z-directed wire, $\omega = 2\pi f$, P_e is power in watts, v is the volume of the

conducting material in cubic meters, w_x is the wire width in the x direction, and w_y is the wire width in the y direction. The losses of (12.18) are sometimes a significant addition to the I^2R losses of the DC resistance.

However, when the skin depth is smaller than the wire radius, then *skin effect losses* are said to occur. The current density distribution is no longer uniform. While the average of the current density J over the wire cross section remains the same, the average power loss density increases. The total power loss is:

$$P = \int \frac{J^2}{\sigma} dv \tag{12.19}$$

Thus skin effect increases power loss, and occurs whenever conductor radius exceeds skin depth. A way to avoid skin effect loss is to replace large conductors by many conductors of much smaller radius, as is done in *Litz wire.* Unfortunately, Litz wire is much more expensive than solid copper or aluminum wire.

Skin effect is usually considered to be associated with the magnetic field of a single isolated wire in air. Because other wires add contributions to the magnetic field, other wires in the proximity cause changes in the power losses. These effects of other wires are included in the *proximity effect.*

Since the magnetic fields are affected by all wires and all magnetic materials, the best way to analyze skin and proximity effects is to use finite-element analysis. The software must include eddy currents and must constrain the total current in each conductor to the same value.

Example 12.2 Skin Effect in an Isolated Conductor A circular copper wire carrying 100 A peak is placed in air, far from any other materials. If its radius is 10 mm, find its current density and magnetic flux density distributions at 400 Hz and 1 Hz using Maxwell. Also find the power loss and resistance per meter.

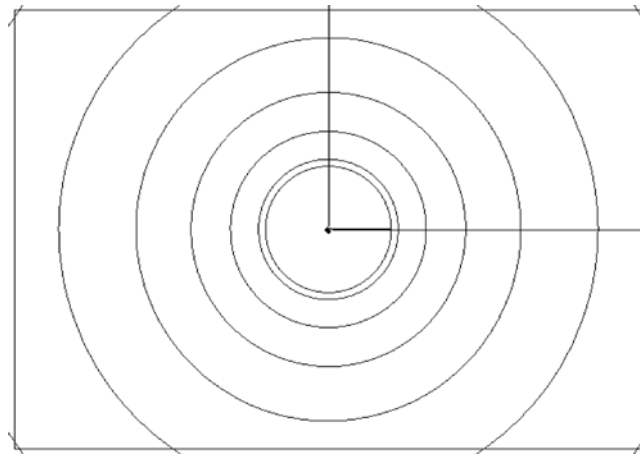

FIGURE E12.2.1 Computer display of computed flux lines in isolated wire at 400 Hz.

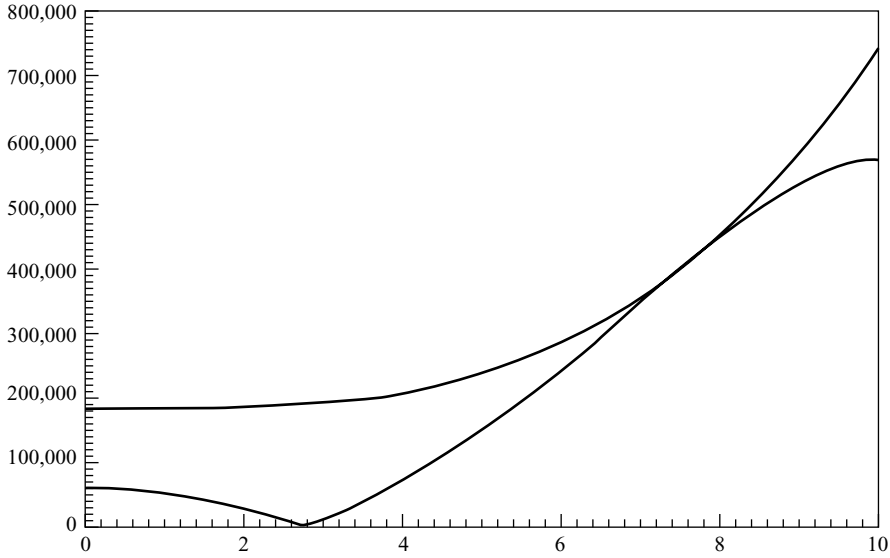

FIGURE E12.2.2 Computed current density at 400 Hz versus radius from center of wire. The upper curve is the total magnitude, and the lower curve is the magnitude at phase angle zero.

Solution Use Maxwell's "Eddy Current" solver with the wire centered in its default model area, placing "balloon" boundaries around the area. At 400 Hz the power loss computed is 0.49036 W/m. Thus the 400-Hz resistance $R = P/I^2$, where I is rms, is 0.98072E−4 Ω/m. Figure E12.2.1 shows the computed flux lines; note that they appear to be concentrated near the wire surface. Figure E12.2.2 graphs the computed current density versus wire radius. Note that the current density decays exponentially from the surface, as expected for an isolated wire. Since the skin depth at 400 Hz from (12.17) is 3.304 mm, the decay over the 10-mm radius appears reasonable.

At 1 Hz, the computed power loss is reduced to 0.2758 W/m. Thus the 1-Hz resistance is 0.5516E−4 Ω/m, which agrees closely with the DC resistance of 0.5488 Ω/m obtained by (12.2). Thus the resistance at 400 Hz is approximately 1.8 times the DC resistance. Graphing the current density versus radius shows an essentially uniform current density throughout the wire at 1 Hz.

Example 12.3 Skin and Proximity Effects in Stator Coil with Clapper An axisymmetric copper coil is placed in a ferrite "cup core" inductor shown in Figure E12.3.1 as created in Maxwell's default drawing area. The area is assumed to confine the flux. The ferrite in the lower stator and upper clapper armature has a relative permeability of 1000 and conductivity of 0.01 S/m. The coil has three copper conductors, each of radius 4 mm and carrying 50 A 400 Hz. Use Maxwell to find the power loss, flux line plot, and current density distribution, showing skin and proximity effects in the three wires.

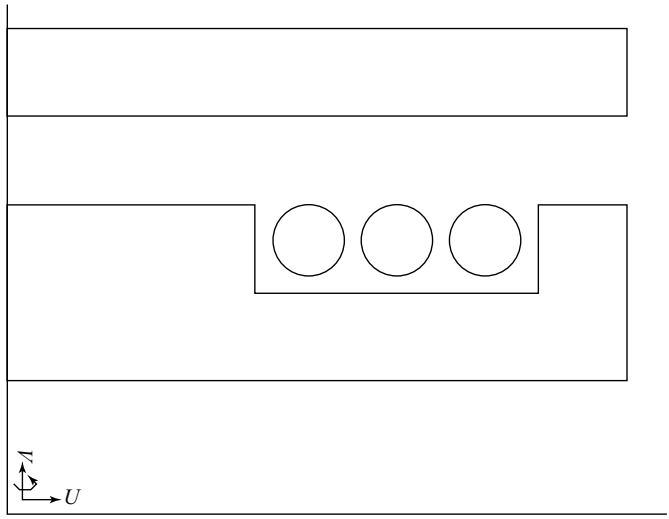

FIGURE E12.3.1 Three-turn winding in ferrite cup core inductor, as drawn in Maxwell's default window. The wire radius is 4 mm.

Solution The model of Figure E12.3.1 was solved by Maxwell's "Eddy Current" solver. The computed power loss is 0.635 W. The flux line distribution is shown in Figure E12.3.2 at phase angle zero. The current density distribution can be plotted in color, but is instead graphed in Figure E12.3.3 along a plane cutting all three wires. Note that each of the three wires has a different current density profile (because each has a different flux density), but all that appear to have the same average current density as they should.

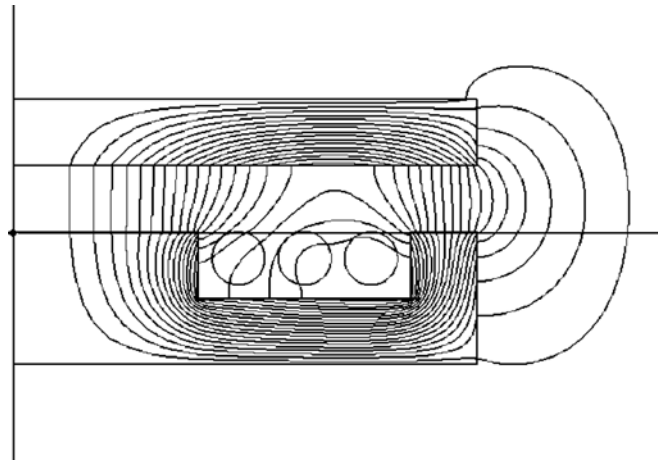

FIGURE E12.3.2 Computer display of flux line plot obtained for Figure E12.3.1.

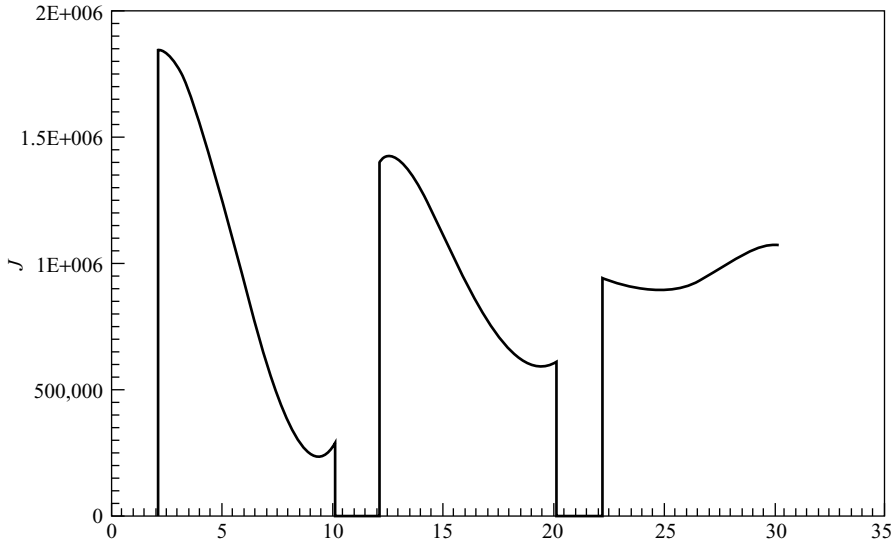

FIGURE E12.3.3 Graph of computed current density J in amperes per square meter versus position along plane cutting through the centers of the three wires in Figure E12.3.1.

12.4 FINITE-ELEMENT COMPUTATION OF TEMPERATURES

As indicated in Figure 12.1, the power losses in magnetic actuators and sensors determine their operating temperature. Since high temperatures can cause device failure and/or fire, it is important to be able to compute temperature distributions.

Thermal computations must in general include three means of heat transfer: conduction, convection, and radiation. This book will examine steady-state thermal computations. Time variation of temperature is studied elsewhere [5,6]. Appendix A includes the symbols, dimensions, and units of heat.

12.4.1 Thermal Conduction

Steady-state thermal conduction is governed by Poisson's differential equation [5,6]:

$$\nabla \cdot k \nabla T = -\frac{P}{v} \tag{12.20}$$

where T is temperature, k is thermal conductivity, and the right-hand side is the negative power per unit volume. Thermal conductivities are similar to electrical conductivities in that they vary from high in metals to low in insulators and also vary somewhat with temperature. Approximate room temperature (20°C) values include 400 W/(m °C) for copper and 80 W/(m °C) for typical steel. Heat conduction is compared with electric and magnetic circuits in Figure 3.2.

There is an analogy between (12.20) and one of Maxwell's equations of Chapter 2. Replacing the electric flux density of (2.49) by permittivity times electric field intensity E gives:

$$\nabla \cdot \varepsilon \mathrm{E} = \rho_v \tag{12.21}$$

where the right-hand side from Chapter 2 is volume charge density. Replacing **E** by the negative gradient of electric scalar potential ϕ_v of (2.39) gives:

$$\nabla \cdot \varepsilon \nabla \phi_v = -\rho_v \tag{12.22}$$

Note that (12.22) is analogous to (12.20). Permittivity ε replaces thermal conductivity k, volume charge density replaces power per unit volume, and electric scalar potential replaces temperature.

Finite-element analysis of thermal conduction problems is commonplace [6, 7]. Since Maxwell is used elsewhere in this book, its electrostatic solution of (12.22) will be used to solve thermal conduction by analogy.

Example 12.4 Steady Thermal Conduction Computation Using Analogy to Electrostatics An axisymmetric copper coil is surrounded by glastic insulation and a cylindrical steel core as shown in Figure E12.4.1. The thermal conductivities are

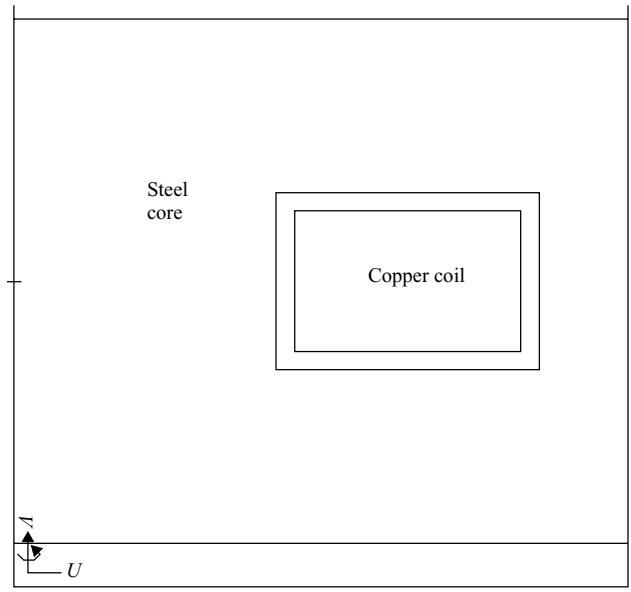

FIGURE E12.4.1 Axisymmetric inductor of radius 70 mm and height 60 mm. The temperature distribution is to be computed when there are power losses in the steel and in the copper coil of size 26 mm radially and 16 mm high, surrounded by glastic insulation 2 mm thick on all sides.

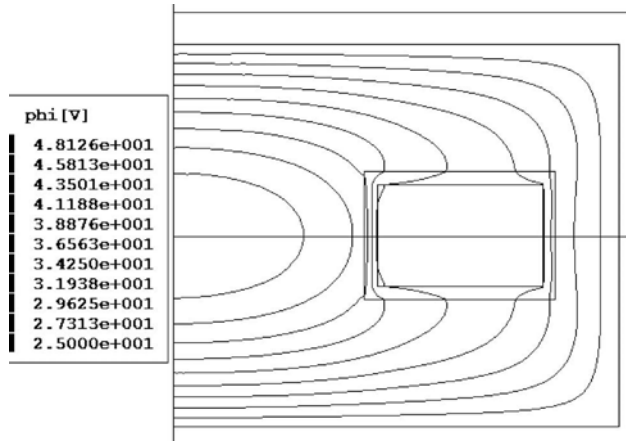

FIGURE E12.4.2 Computer display in black and white of computed voltage contours in inductor of Figure E12.4.1, also available in color. Since voltage is here analogous to temperature, the maximum temperature is approximately 48°C.

400, 10, and 79 W/(m °C), respectively. The copper power loss density is 8000 W/m^3 and the steel core loss density is 4000 W/m^3. Use Maxwell's electrostatic solver to compute the temperature distribution, assuming that the outermost steel of the cylinder is at 25°C.

Solution The relative permittivities to be entered are the above thermal conductivities divided by free space permittivity 8.854E−12. Under "Sources and Boundary Conditions" in Maxwell SV (or under "Excitations" in Maxwell version 16) enter the charge densities of 8000 C/m^3 in the copper coil and 4000 C/m^3 in the steel core; then enter 25 V for the upper, lower, and outer steel boundaries. The computed voltage contours are shown in Figure E12.4.2. Note that the maximum contour value is approximately 48 V in the steel along the axis of symmetry. Thus the maximum temperature is 48°C. Alternatively, thermal finite-element software can be used to also obtain 48°C.

12.4.2 Thermal Convection and Thermal Radiation

Besides thermal conduction, thermal convection and thermal radiation are usually very important in determining temperatures of magnetic actuators and sensors. The easiest way to analyze them is to use the film coefficient h defined by:

$$Q = hA\Delta T \tag{12.23}$$

where Q is heat flow, A is the area of the surface, and ΔT is the temperature difference across the convective and/or radiative region. In many cases ΔT is the temperature rise above the temperature of the surroundings, called the ambient temperature. The coefficient h has SI units of W/(°C m^2).

While the film coefficient varies tremendously with the available airflow paths and temperatures, a value often assumed is 10 W/(°C m^2) for *free convection and radiation*. Free convection is without fan cooling, while *forced convection* has a fan or wind. For more accurate determination of the convection portion of film coefficient h, computational fluid dynamics (CFD) can be carried out, often using finite-element fluid analysis [6].

Thermal radiation is usually proportional to the fourth power of surface absolute temperature [6] in SI units of kelvin (see Appendix A). However, even at surface temperatures common to magnetic actuators and sensors, say 60°C, the portion of film coefficient h due to radiation can be more than that of free convection. Radiation heat transfer is also determined by surface emissivity and geometric view factors [6]. Since both convection and radiation are commonly nonlinear functions of temperature, nonlinear film coefficient h is often required in thermal finite-element computations [7].

Thermal finite-element software is widely available. Maxwell automatically includes electromagnetic power losses in its thermal computations when linking to compatible thermal or computational fluid dynamics software.

12.4.3 AC Magnetic Device Cooled by Conduction, Convection, and Radiation

As an example of temperature computation in laminated magnetic devices, consider the three-phase inductor shown in Figure 12.2. It has a core made of laminations of Armco M6 grade steel of thickness 0.356 mm. To maintain inductance at frequencies above 60 Hz, the laminations are considerably thinner than the 0.635 mm thickness commonly used for 60-Hz laminations. The laminations are stacked to form a core of height of 190.5 mm.

The laminated core material has a B–H curve and core loss curves provided by Armco. To model the core loss using Maxwell's thermal finite-element solver, the Armco core loss curves are fitted to the core loss equation [8, 9]:

$$p = K_h B^2 f + K_c (Bf)^2 + K_e (Bf)^{1.5} \tag{12.24}$$

where p = power loss density in watts per cubic meter, K_h = hysteresis coefficient, K_c = classical eddy current coefficient, K_e = excess (or anomalous) eddy current coefficient due to domains, B = peak magnetic flux density in teslas, and f = frequency in Hz. For the Armco steel laminations used, least-squares curve fitting gives K_h = 66.9, $K_c = 0.210$, and $K_e = 1.92$.

To reduce high frequency losses in the copper windings of the three-phase inductor, the winding turns are made of multiple strands. Figure 12.3 shows the three-phase windings, one on each arm of the laminated core. Each phase has seven turns made of eight strands of octagonal wire. The overall lamination width is 302 mm and the total height (including the top "I" core segment) is 361 mm. The geometry of Figure 12.3 was developed as an Autocad® DXF file, which was then directly input into Maxwell.

FIGURE 12.2 Photograph of laminated three-phase 425-A rms 88-μH inductor for which temperatures are to be found.

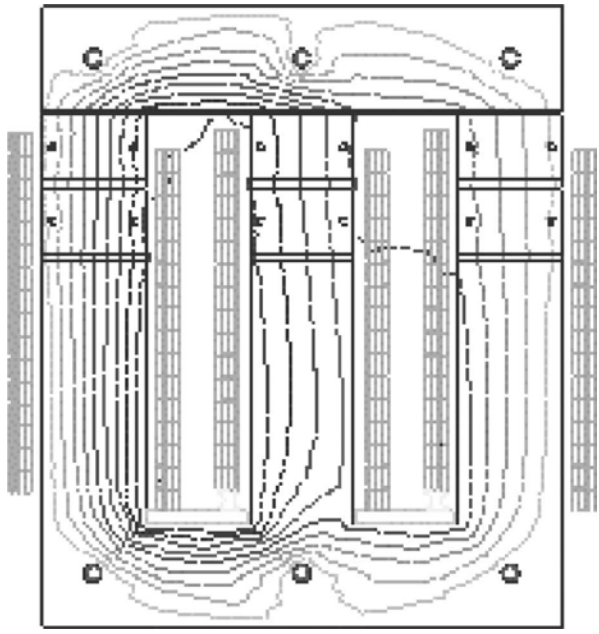

FIGURE 12.3 Computer display of geometry of laminated three-phase inductor, also showing computed magnetic flux lines at time zero, when 14.14 A (10-A rms) of frequency 100 Hz flows in the leftmost winding. Note that there are eight-core segments.

Besides the core and copper losses, losses may occur in the bolts holding the laminations together. The bolts are made of solid steel with a *B–H* curve and electrical conductivity (2.E6 S/m) assumed for SAE 1010 steel.

The three-phase laminated inductor of Figures 12.2 and 12.3 was input to Maxwell, which was used to compute its electromagnetic performance followed by its thermal performance. The magnetic flux density distribution and related electrical parameters and losses were computed over a wide range of current amplitudes and frequencies. Figure 12.3 shows a typical computed magnetic flux line pattern.

The loss distributions in the various copper windings, the various segments of the steel core, and the steel bolts, were computed for frequencies ranging from 1 Hz to 20 kHz. Skin effects and proximity effects in the stranded copper windings were included in the computations. To check the copper loss computation of 0.0507 W at 1 Hz and 10 A rms, the simple DC resistance formula (12.2) was used where length $l = 0.1905$ m, electrical conductivity $\sigma = 5.8\text{E}7$ S/m for Cu, and S_c is the area of the octagonal-shaped strand. Substituting the area and multiplying by I^2 gives a loss of 0.050 W, agreeing closely with the 0.0507 W computed by finite elements.

At higher frequencies for the same 10-A current, finite-element computations show that the copper loss increases from 1.184 W at 100 Hz to 32.266 W at 20 kHz. The increase is due to skin and proximity effects, which also cause changes in the magnetic field flux pattern shown in Figure 12.4 at 4 kHz, which differs in the winding area from Figure 12.3.

The inductance was also computed, which for 60-Hz currents below 750 A was 89.8 μH. This agrees reasonably well with the manufacturer's rated 88 μH and measured 60-Hz inductance of approximately 96 μH at low currents; the small difference is believed due at least in part to the inductance of the leads. Because of skin effects within steel laminations, inductance is expected to be greatly reduced at frequencies 20 kHz and higher [10].

Next, the losses computed were used in a thermal finite-element model, again using the Maxwell SV software. The thermal model is made from the electromagnetic model by adding the necessary thermal materials, boundary conditions, and excitations.

The thermal material properties include the thermal conductivities. Even though the steel used is laminated, the thermal conductivity for solid steel was used; this is believed appropriate since most heat is expected to flow in the *xy* plane of the laminations. Other key thermal conductivities include 10.2 W/(m °C) for the glastic insulation in the "airgaps" between the eight-core segments.

The thermal boundary conditions are convective and radiative, involving a film coefficient. Because the inductor of Figure 12.2 also has available air flow paths at its ends (in the *z* direction out of the figure), the film coefficient assumed here is $h = 15$ W/(°C m^2). The ambient temperature is assumed to be 25°C. The 60-Hz loss distributions were input for 425 A rms. The resulting computed temperature distribution is shown in Figure 12.5.

The maximum computed temperature in Figure 12.5 is 163.5°C, which agrees reasonably well with the measured maximum temperature of 156°C. The computed temperatures are significantly affected by the assumed film coefficient; for example, changing it from 15 W/(°C m^2) to 20 W/(°C m^2) causes the maximum temperature to fall to 145°C.

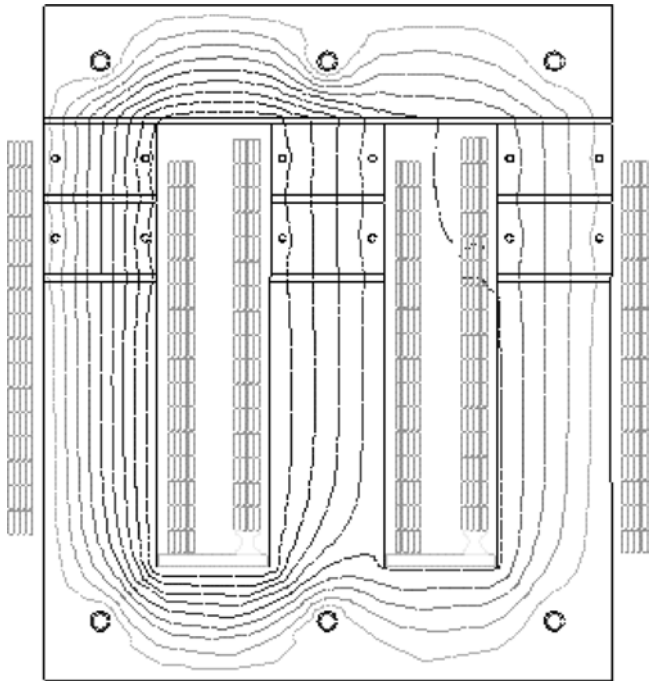

FIGURE 12.4 Computer display of computed flux lines for 14.14 A (10 A rms) of frequency 4 kHz in leftmost winding. Note that due to skin and proximity effects the winding leakage flux lines differ from the low frequency flux lines in Figure 12.3.

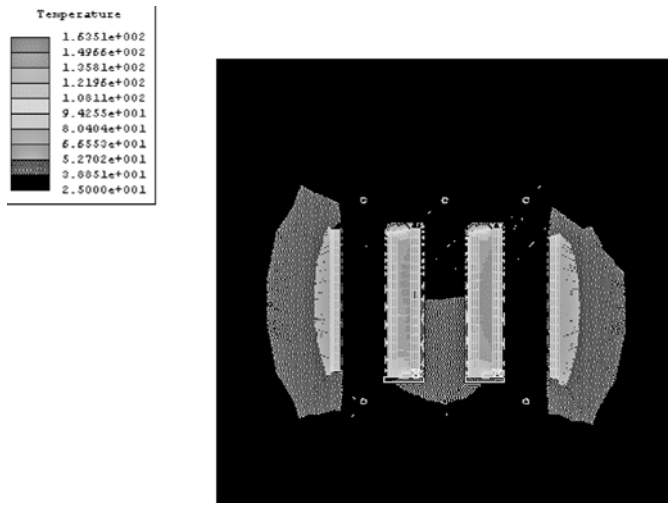

FIGURE 12.5 Computer display in black and white of computed temperature distribution in laminated inductor, also available in color.

PROBLEMS

12.1 Redo Example 12.1 at a temperature of 100°C.

12.2 Redo Example 12.1 when the winding area is increased to 1.5E−3 m^2.

12.3 Redo Example 12.1 when the packing factor is increased to 0.75.

12.4 Redo Example 12.1 when the voltage is increased to 14-V DC.

12.5 Redo Example 12.2 at 60 Hz.

12.6 Redo Example 12.2 with the wire made of aluminum of electrical conductivity 3.54E7 S/m.

12.7 Redo Example 12.3 at 60 Hz.

12.8 Redo Example 12.3 with the wires made of aluminum of electrical conductivity 3.54E7 S/m. Find the power lost in each of the three wires as well as the total loss.

12.9 Redo Example 12.4 with the power loss density doubled in the coil.

12.10 Redo Example 12.4 with the power loss density doubled in the steel core only.

12.11 Redo Example 12.4 with the power loss density doubled in both the coil and the core.

12.12 Redo Example 12.4 with the thermal conductivity of the insulation reduced to 4 W/(m °C).

REFERENCES

1. Juds MA. *Notes on Solenoid Design*, Milwaukee, WI: Eaton Corporate R&D; 2012.
2. Flanagan WM. *Handbook of Transformer Design and Applications*, 2nd ed. New York: McGraw-Hill, Inc.; 1993.
3. Bessho K, Yamada S, Kanamura Y. Analysis of transient characteristics of plunger type electromagnets. *Electr Eng Jpn* 1978;98:56–62.
4. Brauer JR, Ruehl JJ, Hirtenfelder F. Coupled nonlinear electromagnetic and structural finite element analysis of an actuator excited by an electric circuit. *IEEE Trans Magn* 1995;31:1861–1864.
5. Holman JP. *Heat Transfer*. New York: McGraw-Hill Book Co.; 1963.
6. Brauer JR (ed.). *What Every Engineer Should Know About Finite Element Analysis*, 2nd ed. New York: Marcel Dekker, Inc.; 1993, Chapter 4 “Thermal Analysis” by V. D. Overbye and Chapter 5 “Fluid Analysis” by N. J. Lambert.
7. Brauer JR, Wallen P. Coupled 3D electromagnetic, structural, and thermal finite element analysis as integral components of electronic product design, *Proceedings of the IEEE Wescon Conf.*, October 1996, pp. 358–364.

8. Skibinski GL, Schram BG, Brauer JR, Badics Z. Finite element prediction of losses and temperatures of laminated and composite inductors for AC drives, *Proceedings of the IEEE Int. Electric Machines and Drives Conf.*, June 2003.
9. Fitzgerald AE, Kingsley C, Umans SD. *Electric Machinery*, 6th ed. New York: McGraw-Hill Book Co.; 2003.
10. Brauer JR, Beihoff BC, Cendes ZJ, Phillips KP. Laminated steel eddy loss vs. frequency computed using finite element analysis. *IEEE Trans Ind Appl* 2000;36:1132–1137.